Gas-phase phosphorous poisoning of a Pt/Ba/Al2O3 NOx storage catalyst

catalysts

MDPI

Article

Gas-Phase Phosphorous Poisoning of a Pt/Ba/Al_2O_3 NO_x Storage Catalyst

Rasmus Jonsson [1], Oana Mihai [1], Jungwon Woo [1], Magnus Skoglundh [1], Eva Olsson [1], Malin Berggrund [2] and Louise Olsson [1,*]

[1] Competence Centre for Catalysis, Chalmers University of Technology, SE-412 96 Gothenburg, Sweden; rasjon@chalmers.se (R.J.); oana.mihai@chalmers.se (O.M.); jungwon@chalmers.se (J.W.); skoglund@chalmers.se (M.S.); eva.olsson@chalmers.se (E.O.)

[2] Volvo Car Corporation, SE-405 31 Gothenburg, Sweden; malin.berggrund@volvocars.com

* Correspondence: louise.olsson@chalmers.se; Tel.: +46-31-772-4390

Received: 9 March 2018; Accepted: 7 April 2018; Published: 11 April 2018

Abstract: The effect of phosphorous exposure on the NO_x storage capacity of a Pt/Ba/Al_2O_3 catalyst coated on a ceramic monolith substrate has been studied. The catalyst was exposed to phosphorous by evaporating phosphoric acid in presence of H_2O and O_2. The NO_x storage capacity was measured before and after the phosphorus exposure and a significant loss of the NO_x storage capacity was detected after phosphorous exposure. The phosphorous poisoned samples were characterized by X-ray photoelectron spectroscopy (XPS), environmental scanning electron microscopy (ESEM), N_2-physisorption and inductive coupled plasma atomic emission spectroscopy (ICP-AES). All characterization methods showed an axial distribution of phosphorous ranging from the inlet to the outlet of the coated monolith samples with a higher concentration at the inlet of the samples. Elemental analysis, using ICP-AES, confirmed this distribution of phosphorous on the catalyst surface. The specific surface area and pore volume were significantly lower at the inlet section of the monolith where the phosphorous concentration was higher, and higher at the outlet where the phosphorous concentration was lower. The results from the XPS and scanning electron microscopy (SEM)-energy dispersive X-ray (EDX) analyses showed higher accumulation of phosphorus towards the surface of the catalyst at the inlet of the monolith and the phosphorus was to a large extent present in the form of P_4O_{10}. However, in the middle section of the monolith, the XPS analysis revealed the presence of more metaphosphate (PO_3^-). Moreover, the SEM-EDX analysis showed that the phosphorous to higher extent had diffused into the washcoat and was less accumulated at the surface close to the outlet of the sample.

Keywords: LNT; NSR; NO_x storage; phosphorous; deactivation; poisoning

1. Introduction

In diesel and lean burn gasoline engines, the engine operates with a large excess of air, and this results in an increased fuel economy, and thereby reduced emissions of CO_2, which is a greenhouse gas. However, it is critical to remove NO_x, which can be done by different catalytic aftertreatment techniques. Emission standards have therefore been implemented in large parts of the world and the emission levels have been significantly reduced over the years [1].

Since the traditional Three-way catalyst (TWC), requires stoichiometric air:fuel ratio, the Lean NO_x Trap (LNT) was introduced as a catalytic concept for exhaust gas treatment in diesel vehicles [2–5]. In the LNT, usually barium is used as a storage component, and the nitrogen oxides during lean conditions are stored on barium as barium nitrates. Moreover, noble metals, such as platinum, play a key role to oxidize the NO to NO_2, which facilities the NO_x storage [2,6–10]. Under short

periods of time the engine is switched from operating under lean to rich conditions. Under rich conditions, barium nitrates decompose and are reduced over the noble metal sites to mainly N_2 and H_2O. The reducing agents in the exhaust gas are hydrocarbons (HC), carbon monoxide (CO) and hydrogen (H_2), which react with the NO_x to produce CO_2, H_2O and N_2. Nitrogen is the desired product from the reduction of stored nitrates. However, there are other possible bi-products from the reduction process such as ammonia (NH_3) and nitrous oxide (N_2O) [3].

A vehicle is expected to be in service for a long time, which requires the catalyst to be durable. Over time, the catalytic properties of the catalyst deteriorate. There are a few mechanisms that contribute to degradation of catalysts, such as sintering of catalytic particles as a result of high-temperature exposure [11]. The catalytic washcoat can also undergo mechanical tear and poisoning of active sites on the catalyst caused by chemisorption or reactions of catalytically active sites with poisons in the exhaust gas [12]. The poisons are often introduced to the system through the gasoline or diesel fuel, which is the case for SO_2, or through the lubricant of the engine. Lubricants, such as zinc dialkyldithiophosphate (ZDDP), are commonly used in vehicles and are a source for accumulation of both sulfates, zinc and phosphorus in the catalyst [13]. The deactivation effect of sulfur has extensively been studied over LNTs [12,14–16], and also how to regenerate the catalyst from sulfur [17].

There are only a few studies available in the open literature where phosphorus poisoning has been studied over noble metal catalysts used for emission control. Bunting et al. [13] studied a diesel oxidation catalyst (DOC) connected to an engine rig where the fuel was doped with ZDDP, which showed accumulation of foreign compounds such as phosphates, zinc and sulfates on the catalyst. Also, results from characterization of field-aged TWCs showed accumulation of elements found from ZDDP poisoning of catalysts [18–20]. Moreover, it has been shown that the distribution of phosphorus as it accumulates in the catalytic washcoat exhibits a gradient, with higher concentration at the inlet and lower along the washcoat length [19–23]. Compared to sulfur, which has a more even distribution over the washcoat and penetrates deep into the washcoat, phosphorus tends to be more concentrated close to the washcoat surface [13]. A study performed by Galisteo et al. [24], where a $Pt/Ba/Al_2O_3$ catalyst was impregnated with $(NH_4)_2HPO_4$, showed that the amount of phosphorus in the catalyst correlated with the loss of NO_x storage capacity.

However, there are, to our knowledge, no studies in the open literature that have examined phosphorus poisoning of LNT catalysts using vapour phase exposure that is closer to realistic poisoning conditions, which is the objective of the present work. In this study, we have examined a $Pt/Ba/Al_2O_3$ catalyst exposed to phosphorous in the gas phase using different phosphorous concentrations. The catalyst samples were studied in a flow reactor to determine changes in NO_x storage capacity, NO_x reduction activity and bi-product formation. The phosphorous-exposed samples were also characterized by X-ray photoelectron spectroscopy (XPS), nitrogen-physisorption, Inductive coupled plasma atomic emission spectroscopy (ICP-AES) and Environmental Scanning Electron Microscopy (ESEM) with energy dispersive X-ray (EDX) analysis.

2. Results and Discussion

2.1. Activity Measurements

Lean/rich cycling experiments were conducted in which the system was exposed to 400 vol.-ppm NO, 5 vol.-% CO_2, 5 vol.-% H_2O and 8 vol.-% O_2 during the lean phase. In this phase, NO is first oxidized over the platinum sites, and thereafter storage of NO_x species occurs as nitrates through a disproportionation mechanism, but also via nitrite formation at low temperature [5]. The NO oxidation capacity of the catalyst is clearly visible by the NO_2 formation seen in Figure 1. In the initial part of the lean phase, all NO_x is stored and after a certain amount of time, breakthrough of NO_x, due to saturation of the storage sites, is seen. Most NO_x is stored onto the barium sites in form of $Ba(NO_3)_2$, but some NO_x is also stored onto alumina sites [3]. At lower temperature, storage of NO_x occurs over

both the barium and alumina sites, but at higher temperature the barium sites dominate the NO_x storage [25], due to the lower stability of alumina nitrates.

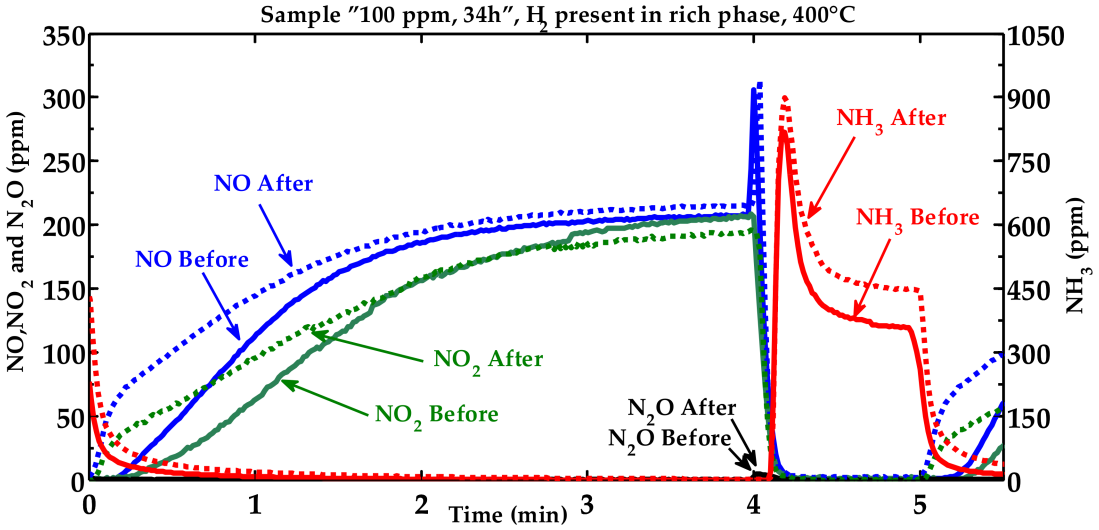

Figure 1. Measured outlet NO, NO_2, N_2O and NH_3 concentrations for the $Pt/Ba/Al_2O_3$ sample "100 ppm, 34 h" before and after exposure to phosphorous (100 vol.-ppm H_3PO_4, 8 vol.-% O_2, 5 vol.-% H_2O at 200 °C) in a flow-reactor experiment at 400 °C. Lean phase; 400 vol.-ppm NO, 5 vol.-% H_2O, 5 vol.-% CO_2 and 8 vol.-% O_2. Rich phase; 400 vol.-ppm NO, 5 vol.-%H_2O, 5 vol.-% CO_2 and 1 vol.-% H_2.

As the system is switched from lean to rich phase, a NO_x peak is visible, which is related to release of stored NO_x in the catalytic material [26]. Directly after the switch from the lean to the rich (1 vol.-% H_2, 5 vol.-% CO_2 and 5 vol.-% H_2O) phase, minor formation of N_2O is seen and it is during this short period of time, that most of the N_2 formation is suggested to occur [27–29]. After the N_2O peak a large ammonia peak is observed, which is consistent with the work by Lindholm et al. [25]. Most of the formed NH_3, early in the rich phase, is consumed by a Selective Catalytic Reduction (SCR) reaction with the stored NO_x, according to Lietti et al. [27] and Lindholm et al. [6]. Hence, the NH_3 peak is delayed and will dominate more as the rich phase proceeds and this is also seen in Figure 1. Indeed, spatially resolved MS measurements performed by Partridge et al. [10] showed a clear axial consumption of ammonia.

The effect of phosphorus exposure was studied by exposing the $Pt/Ba/Al_2O_3$ catalyst to 100 vol.-ppm H_3PO_4, 8 vol.-% O_2 and 5 vol.-% H_2O at 200 °C for 34 h and thereafter repeating the same experiment, see Figure 1. In addition, a second catalyst was used, which was exposed to 50 vol.-ppm H_3PO_4 instead. These catalysts were studied under lean/rich cycling experiments, which were conducted both at 300 and 400 °C, using 400 vol.-ppm NO, 5 vol.-% CO_2, 8 vol.-% O_2, and 5 vol.-% H_2O for the lean conditions and 1 vol.-% H_2 or 1000 vol.-ppm C_3H_6, 400 vol.-ppm NO, 5 vol.-% CO_2 and 5 vol.-% H_2O during the rich conditions, and the resulting outlet NO_x concentrations are shown in Figure 2. The results show that exposure to phosphorus causes a significant loss of NO_x storage capacity for the $Pt/Ba/Al_2O_3$ catalyst. The loss of NO_x storage capacity is summarised in Table 1. It is clear that the loss in storage capacity is similar for both poisoning levels and, moreover, that the effect is more pronounced after exposure at 300 compared to 400 °C.

Our results are in line with those in the study by Galisteo et al. [24], where the effect of phosphorous on the NO_x storage capacity of $Pt/Ba/Al_2O_3$ was studied by impregnation of the catalyst with $(NH_3)_3PO_4$ dissolved in water. The authors also observed a decreased NO_x storage capacity after phosphorous exposure. At 300 °C, the NO_x reduction properties of C_3H_6 are poor compared to 400 °C (compare graph B and D in Figure 2), which previously has been observed by

Olsson et al. [30]. However, loss in NO_x storage capacity is still observed for this case after phosphorus exposure. For exposure at 400 °C, the phosphorus poisoning is similar for both H_2 and C_3H_6, which indicates that as long as the reductant can remove the NO_x, the phosphorus poisoning is related to poisoning of the reactions under lean conditions. For phosphorous exposure at 300 °C on the other hand, the reduction with propene is poor, which results in low NO_x storage and therefore the effect of phosphorus poisoning is not seen equally clear.

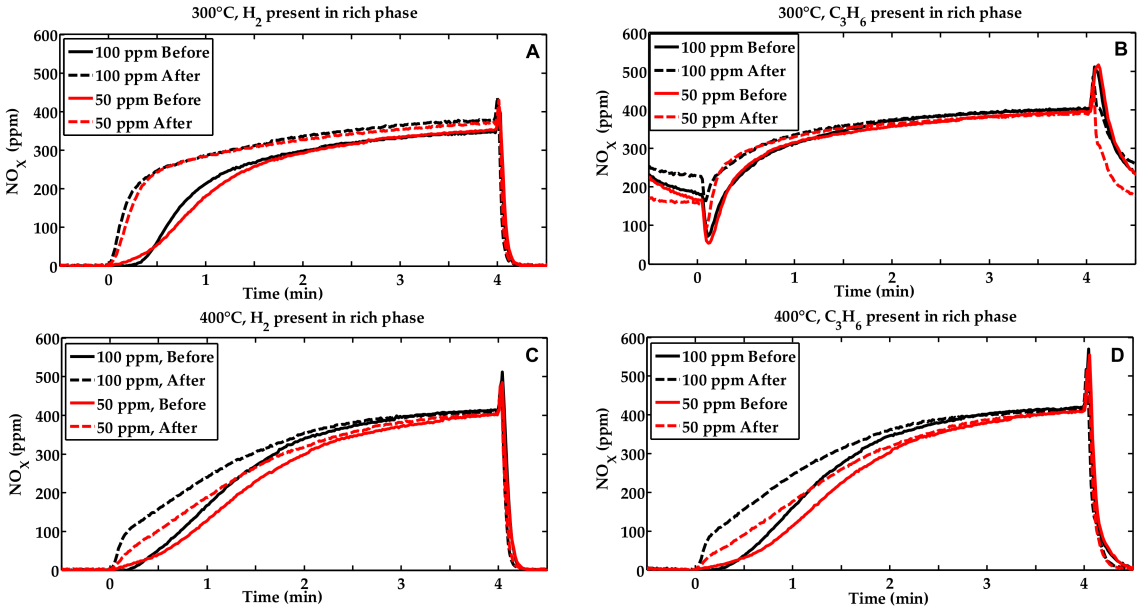

Figure 2. Measured outlet NO_x before and after exposing $Pt/Ba/Al_2O_3$ to 50 or 100 vol.-ppm H_3PO_4, 8 vol.-% O_2 and 5 vol.-% H_2O for 34 h. The lean phase (400 vol.-ppm NO, 5 vol.-% H_2O, 5 vol.-% CO_2 and 8 vol.-% O_2) starts at time = 0. The rich phase consist of 400 vol.-ppm NO, 5 vol.-% H_2O, 5 vol.-% CO_2 and H_2 or C_3H_6, where (**A**) 300 °C with 1 vol.-% H_2 in the rich phase, (**B**) 300 °C with 0.1 vol.-% C_3H_6 in the rich phase, (**C**) 400 °C with 1 vol.-% H_2 in the rich phase, and (**D**) 400 °C with 0.1 vol.-% C_3H_6 in the rich phase.

Table 1. NOx storage capacity for fresh and phosphorous exposed samples.

Condition	NO_x Storage Capacity (µmol)	Loss in NO_x Storage Capacity (µmol)
$NO+H_2$, 300 °C, fresh	92.4	-
$NO+H_2$, 300 °C, 50 ppm P	56.2	36.2
$NO+H_2$, 300 °C, fresh	88.8	-
$NO+H_2$, 300 °C, 100 ppm P	51.4	37.4
$NO+H_2$, 400 °C, fresh	85.9	-
$NO+H_2$, 400 °C, 50 ppm P	70.6	15.3
$NO+H_2$, 400 °C, fresh	70.3	-
$NO+H_2$, 400 °C, 100 ppm P	51.5	18.8

The resulting N_2O formation during these experiments is shown in Figure 3, and it is observed that the selectivity towards N_2O is higher at low temperatures, which is in accordance with the literature [31]. Most of the N_2O is formed in the first part of the rich period, but also a peak in the beginning of the lean phase is observed. Choi et al. [32] found that the second N_2O peak relates to reactions with NH_3. When shifting from rich to lean phase, the formation of NH_3 ceases due to the replacement of H_2 with O_2 in the feed. Therefore, it is plausible that the second N_2O peak relates to consumption of stored NH_3 to form N_2O.

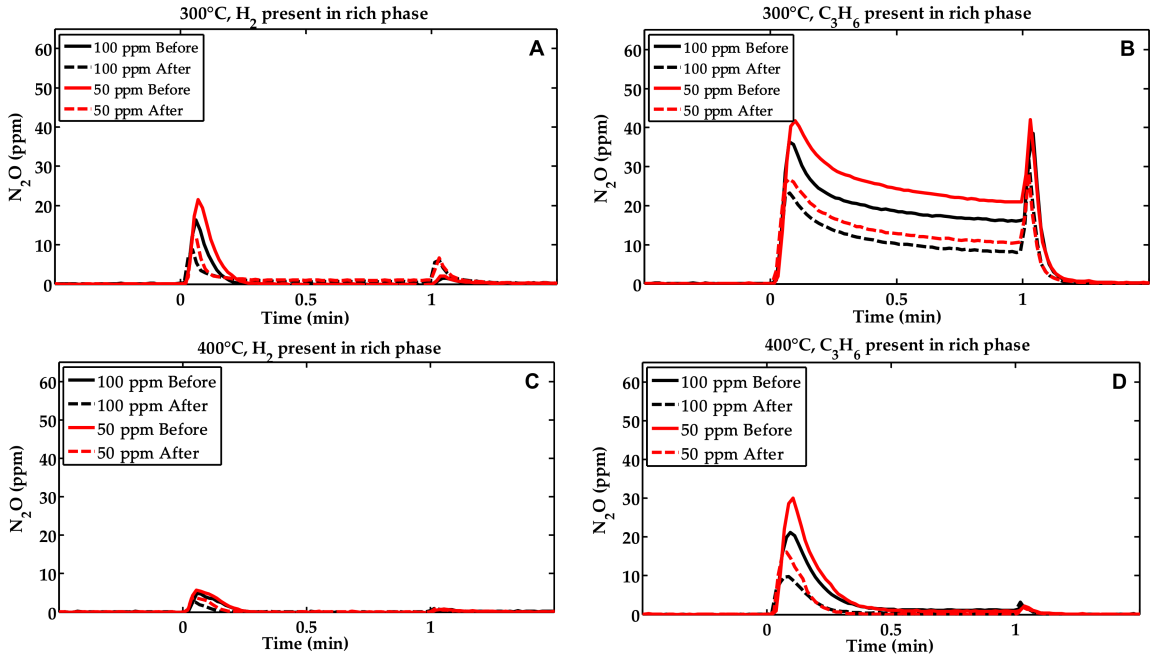

Figure 3. Measured outlet N_2O before and after exposing $Pt/Ba/Al_2O_3$ to 50 or 100 vol.-ppm H_3PO_4, 8 vol.-% O_2 and 5 vol.-% H_2O for 34 h. The rich phase (400 vol.-ppm NO, 5 vol.-% H_2O, 5 vol.-% CO_2 and H_2 or C_3H_6) starts at time = 0. The lean phase consist of 400 vol.-ppm NO, 5 vol.-% H_2O, 5 vol.-% CO_2 and 8 vol.-% O_2, where (**A**) 300 °C with 1 vol.-% H_2 in the rich phase, (**B**) 300 °C with 0.1 vol.-% C_3H_6 in the rich phase, (**C**) 400 °C with 1 vol.-% H_2 in the rich phase, and (**D**) 400 °C with 0.1 vol.-% C_3H_6 in the rich phase.

In addition, more N_2O is formed when using propene as the reducing agent compared to hydrogen. The N_2O formation was previously studied by Olsson et al. [30] where a kinetic model for the reduction of NO_x by C_3H_6 was developed. The reason for the N_2O formation is the reaction between the hydrocarbon and NO_x to form N_2O [33]. Furthermore, in the beginning of the lean phase after propene reduction, there is an increase in the N_2O formation. This is due to reaction between NO_x and HC species, stored during the rich phase. In addition, the results clearly show that the formation of N_2O in the rich phase decreases after exposure to phosphoric acid. The decrease in N_2O formation occurs at both 300 and 400 °C for both H_2 and C_3H_6 as the reducing agent. When comparing the ratio of (N_2O formed)/(NO_x stored) at 300 °C with propene as reductant, the ratio clearly decreases after phosphorous exposure (0.015, 0.0084, 0.020 and 0.011 for first sample before and after exposure for 100 vol.-ppm P, and for second sample before and after exposure for 50 vol.-ppm P, respectively). Thus, it is clear that the N_2O formation not decreases only due that less NO_x is stored, but also due to that the selectivity changes because of the poisoning. De Abreu Goes et al. [11] studied thermal exposure of LNT catalysts, which resulted in sintering of the catalytic particles that in turn resulted in decreased formation of N_2O. Since the catalyst in the present study was not exposed to high temperature again after the degreening step, sintering as a cause for the loss of N_2O formation is not likely. Therefore, the reduced N_2O formation after phosphorous exposure is more likely to relate to poisoning of the platinum sites.

With H_2 as the reducing agent, the formation of NH_3 is higher compared to C_3H_6 as reductant, which can be seen in Figure 4. At 300 °C, the formation of NH_3 is even negligible for the C_3H_6 case. For both samples, the NH_3 formation is slightly higher after the exposure to phosphorus when H_2 is used as the reducing agent. The ammonia formed over the LNT depends on several reactions occurring simultaneously: (i) ammonia production from inlet NO_x; (ii) ammonia production from stored NO_x; and (iii) reaction of the formed ammonia with stored NO_x in an SCR process [6]. An increase in the

ammonia production has also been observed for field-aged, oven-aged and sulphur-poisoned LNT catalysts [11,34]. The reason for the increase in ammonia formation after phosphorus exposure could be related to the loss of NO_x storage capacity depicted in Figure 2. Since less NO_x is available in the form of nitrates during the lean phase, less ammonia can in turn react in the SCR reaction with the stored nitrates [6], and thereby the ammonia release is higher. However, less ammonia will also be produced from the stored NO_x, thus this means that the SCR reaction is more influenced by the phosphorous poisoning compared to the ammonia production. The increased ammonia production during rich conditions can be beneficial for the cases where an SCR catalyst is placed downstream of the LNT [8], in the so-called passive SCR technique.

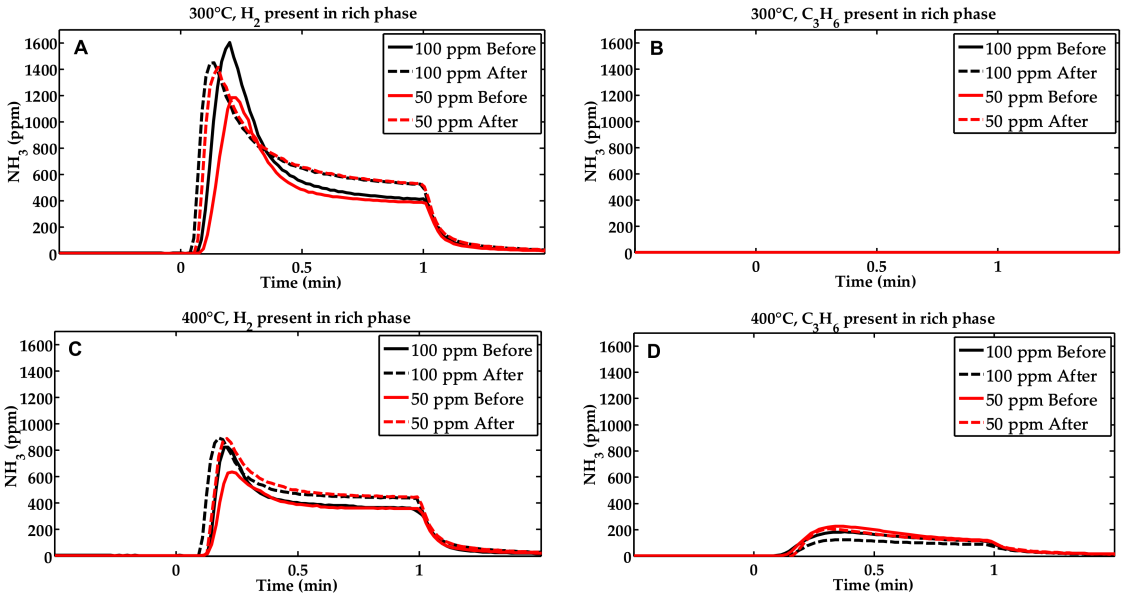

Figure 4. Measured outlet NH_3 concentration before and after exposing $Pt/Ba/Al_2O_3$ to 50 or 100 vol.-ppm H_3PO_4, 8 vol.-% O_2 and 5 vol.-% H_2O for 34 h. The rich phase (400 vol.-ppm NO, 5 vol.-% H_2O, 5 vol.-% CO_2 and H_2 or C_3H_6) starts at time = 0. The lean phase consist of 400 vol.-ppm NO, 5 vol.-% H_2O, 5 vol.-% CO_2 and 8 vol.-% O_2, where (**A**) 300 °C with 1 vol.-% H_2 in the rich phase, (**B**) 300 °C with 0.1 vol.-% C_3H_6 in the rich phase, (**C**) 400 °C with 1 vol.-% H_2 in the rich phase, and (**D**) 400 °C with 0.1 vol.-% C_3H_6 in the rich phase.

The outlet N_2 concentration was not measured due to IR spectroscopy was used for the gas phase analysis. By assuming that all nitrogen leaving the catalyst are either in form of NO, NO_2, NH_3, N_2O or N_2, the remaining N_2 can be determined. The quantities of NO_x, NO, NO_2 NH_3 and N_2O were estimated by integration of the data from the FTIR analysis. The results from these calculations are shown in Figure 5 and it is clear that the formed amount of N_2 is quite low. The reason for this is that we intentionally used long lean and rich cycles to come closer to saturation and also more complete regeneration. In a real application, the cycle times would be different, giving a high amount of N_2. Moreover, the results clearly show a minor N_2O formation in all conditions except with C_3H_6 as reducing agent at 300 °C. Hence, the main difference between the results from the different experimental conditions is the formation of NH_3, N_2 and release of NO_x. The phosphorous-exposed samples tend to release higher amounts of NO_x and NH_3 at the cost of formation of the desired product; N_2. According to the ICP-AES results shown in Table 2, the amount of accumulated phosphorous is similar for both H_3PO_4 concentrations. Thus the H_3PO_4 concentration does not seem to be such a critical factor for the poisoning at these levels. Therefore, the difference before and after phosphorous exposure between the two cases appears similar. For H_2 as the reducing agent, exposure to phosphorus has a more pronounced effect at 300 than 400 °C. The reason for this could be that since the ammonia

production is higher at lower temperature, and is to a large extent influenced by the phosphorous poisoning, it results in a more pronounced effect on the N_2 selectivity. However, for C_3H_6 as the reducing agent, there is no clear trend regarding the selectivities between the fresh and phosphorous exposed samples at 300 and 400 °C. The reason for this could be that the amounts of NH_3 and N_2O formed in these experiments are low, so most of the species are NO_x and N_2.

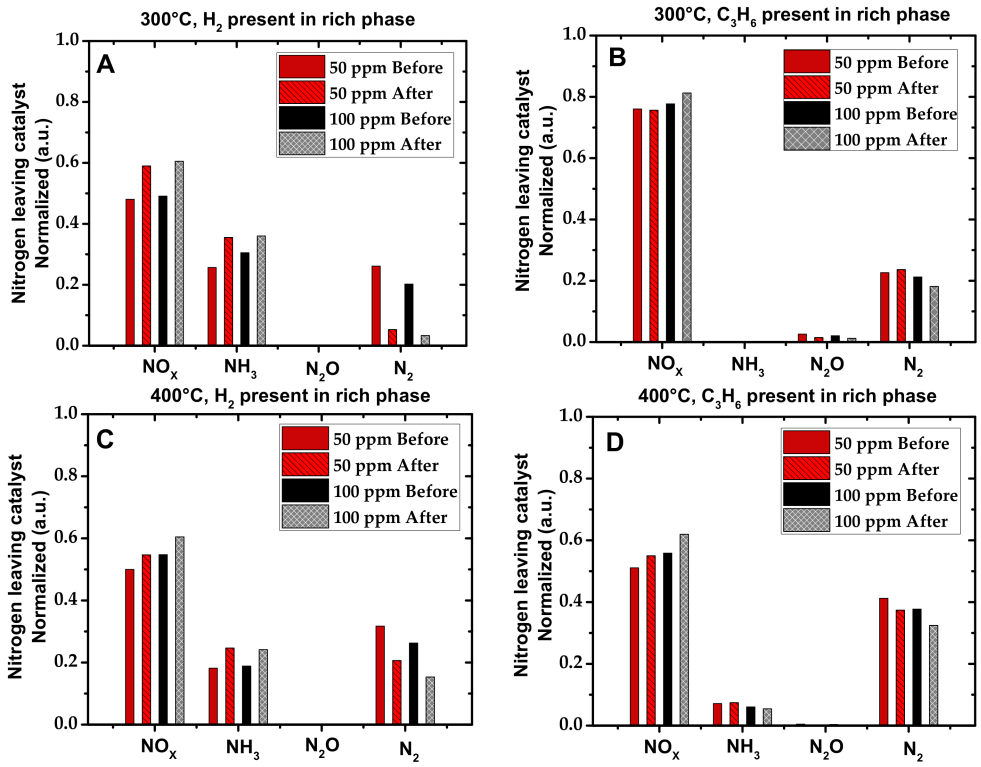

Figure 5. Balance over outlet nitrogen atoms over a lean/rich cycle before and after exposing $Pt/Ba/Al_2O_3$ to 50 and 100 vol.-ppm H_3PO_4 for 34 h, assuming that all nitrogen leaving the catalyst is either in form of NO_x, NH_3, N_2O or N_2. (**A**) 300 °C with 1 vol.-% H_2 in the rich phase, (**B**) 300 °C with 0.1 vol.-% C_3H_6 in the rich phase, (**C**) 400 °C with 1 vol.-% H_2 in the rich phase, (**D**) 400 °C with 0.1 vol.-% C_3H_6 in the rich phase.

2.2. Characterization of the Phosphorous Exposed Samples

One channel of the phosphorous-exposed monolith sample "50 ppm, 34 h" was cut out and the surface composition in the inlet, middle, and in the outlet section of the channel was analyzed by XPS. The overall spectra (see Figure 6A), show that the magnitude of the phosphorus peaks is highest from the surface of the inlet section and lowest from the outlet section of the phosphorous exposed sample. The P 2p binding energy region measured with higher resolution for the inlet and outlet sections for the phosphorous exposed sample are shown in Figure 6B. Due to different signal intensities from the two samples, the spectra are normalized to facilitate the interpretation of the peak positions when comparing different spectra with each other. The intensity of the P 2p peak from the middle section of the sample is significantly lower compared to the peak from the inlet section. In addition, the results show that the position of the P 2p peak shifts towards lower binding energy for the middle section compared to the inlet section of the sample. Deconvolution of the P 2p peak for the inlet and middle section of the sample can be seen in Figure 7. For the inlet section of the sample the deconvolution shows a higher presence of P_4O_{10} with a binding energy ranging between 135.0 and 135.5 eV [35]. However, for the middle region of the sample, the deconvolution shows that metaphosphates, PO_3^-, dominate, which have a binding energy ranging between 134.0 and 134.5 eV [35]. Formation of

metaphosphates has previously been observed after exposing Cu/BEA [36] as well as Fe/BEA [37] for phosphoric acid in gas phase. In addition, formation of P_4O_{10} was also found on Fe/BEA [37], which is in line with our observations. Our results show that the phosphorus-containing surface species mainly are in the form of P_4O_{10} in the inlet section of the sample, where the phosphorus concentration and deposition is higher, while in the middle section more metaphosphates are seen.

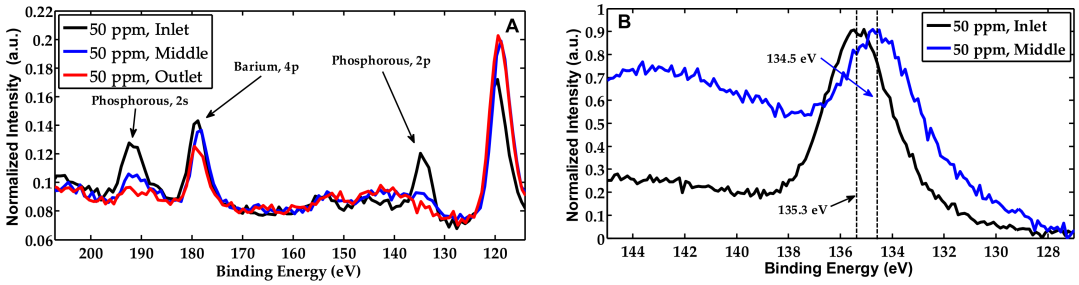

Figure 6. (**A**) Normalized X-ray photoelectron spectroscopy (XPS) spectra from the inlet, middle and outlet section of the $Pt/Ba/Al_2O_3$ sample exposed to 50 vol.-ppm H_3PO_4 for 34 h. (**B**) Corresponding XPS spectra for the P 2p region from the inlet and middle section of the sample.

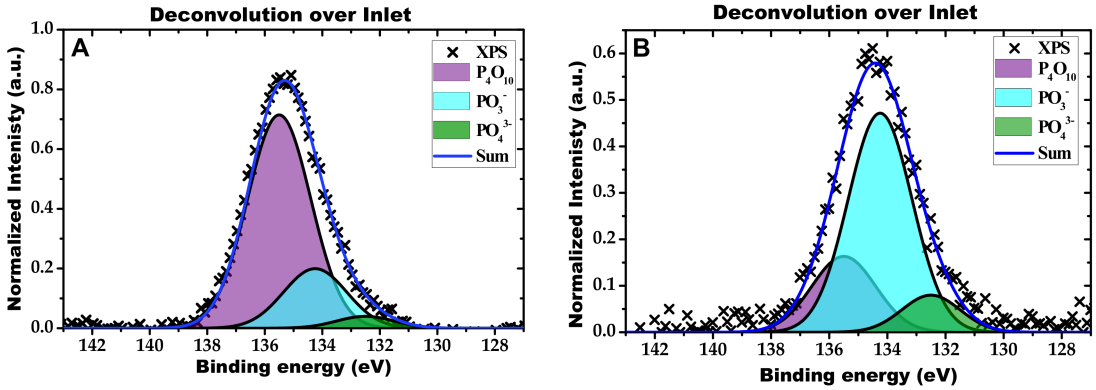

Figure 7. Deconvolution of the P 2p XPS spectra from the inlet (**A**) and middle (**B**) section of the $Pt/Ba/Al_2O_3$ sample exposed to 50 vol.-ppm H_3PO_4 for 34 h. The considered phosphorous species are P_4O_{10}, PO_3^- and PO_4^{3-}.

In order to achieve further insight into the effect of phosphorous exposure in the axial direction of the $Pt/Ba/Al_2O_3$ catalyst, the specific surface area and pore volume, and elemental composition of the inlet, middle and outlet sections of the samples exposed for 100 and 50 vol.-ppm phosphorous for 34 h were analysed together with a degreened sample. In Table 2, the phosphorus content from ICP-AES analysis is presented along with the specific surface area and pore volume. The results show that phosphorus has a gradient distribution, from the inlet to the outlet section of the two phosphorous-exposed samples, which is in line with other studies of both field-aged catalysts and experiments in engine rigs [13,19–23,38,39]. Moreover, it is found that the effect of the phosphorus concentration is minor, which is in line with the flow reactor experiments. Glisteo et al. [24] impregnated a $Pt/Ba/Al_2O_3$ catalyst with aqueous solutions of phosphorous of different concentrations. Their results showed that the specific surface area decreased more by higher phosphorous concentration accumulated on the catalyst, which is in line with our results. We find that the phosphorus content is the highest, and the surface area and pore volume have lowest values, for the inlet section of both catalysts exposed to phosphorous. Close to the outlet section, the phosphorus content is much lower for both samples, whereas the specific surface area and pore volume are higher and more similar to the degreened sample.

Table 2. Phosphorous content, specific surface area and pore volume of the fresh $Pt/Ba/Al_2O_3$ sample and of the $Pt/Ba/Al_2O_3$ samples exposed to 50 and 100 vol.-ppm phosphorous for 34 h. The phosphorus contents are measured by inductive coupled plasma atomic emission spectroscopy (ICP-AES).

	P-content, (wt.-%)	S_{BET} (m^2/(g washcoat)) [1]	V_P (cm^3/(g washcoat)) [1]
Fresh	-	134	0.46
50 ppm, 34 h, inlet	2.2	98	0.36
50 ppm, 34 h, middle	0.40	130	0.45
50 ppm, 34 h, outlet	0.11	134	0.45
100 ppm, 34 h, inlet	2.0	113	0.35
100 ppm, 34 h, middle	0.38	123	0.39
100 ppm, 34 h, outlet	0.07	132	0.39

[1] Estimated based on washcoat amount.

The results from ESEM and EDX analyses acquired from two different positions; 2 mm from the front and 2 mm from the back of the monolith sample exposed for 50 vol.-ppm phosphorous for 34 h are presented in Figures 8 and 9, respectively. Besides phosphorus, other elements (Al and Ba) that are present in the washcoat are depicted in the images. Moreover, silicon, which is one of the major compounds of the cordierite substrate, is also shown. The analysis 2 mm from the front of the sample (Figure 8) indicates that phosphorus is located towards the surface of the washcoat, which previously has been shown for catalysts exposed to ZDDP doped fuel in engine rigs [13]. Closer to the outlet of the sample, less phosphorus is present and the distribution of the phosphorus is more uniform in the washcoat. Accumulation of phosphorus towards the front of the catalyst has been shown for field-aged catalysts [21]. The ESEM-EDX results in the present study can be related to the XPS results (Figure 7), which showed more P_4O_{10} in the inlet section of the sample, while more metaphosphates in the middle section of the phosphorous exposed sample. Finally, in the outlet section of the monolith sample, only small amounts of phosphorus are observed with EDX, but it should be noted that phosphorus is still visible, which means that in a catalytic aftertreatment system it is possible that a catalyst placed downstream the NO_x storage catalyst also can be exposed to phosphorus.

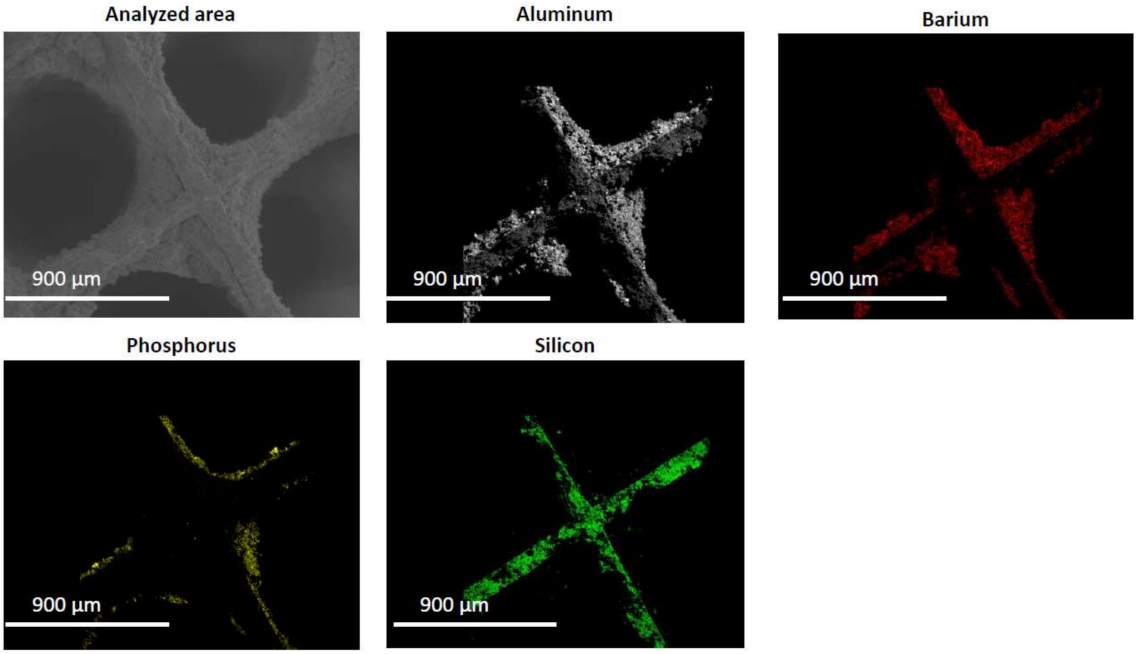

Figure 8. Environmental scanning electron microscopy (ESEM) and energy dispersive X-ray (EDX) images from the cross-section 2 mm from the front of the $Pt/Ba/Al_2O_3$ sample exposed to 50 vol.-ppm H_3PO_4 for 34 h.

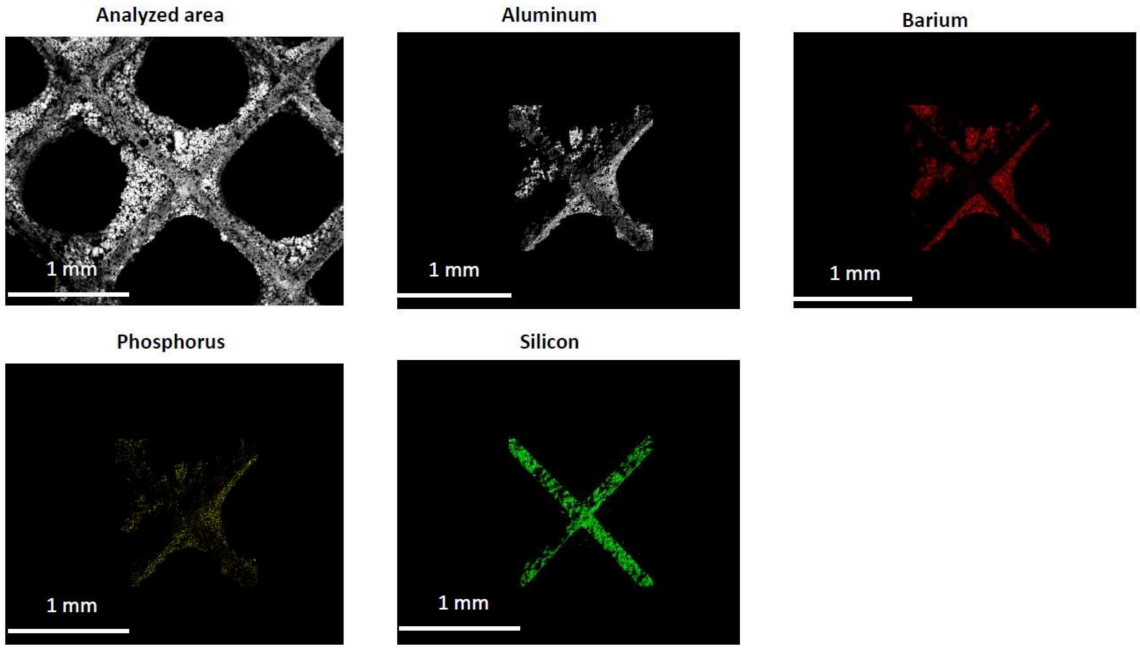

Figure 9. ESEM and EDX images from the cross-section 2 mm from the back of the $Pt/Ba/Al_2O_3$ sample exposed to 50 vol.-ppm H_3PO_4 for 34 h.

To summarize, the combined XPS, EDX, BET and ESEM-EDX data suggest that during phosphorus exposure in the vapour phase more phosphorus is deposited in the inlet of the monolith sample and this phosphorous is mainly located at the surface of the washcoat and contains a large fraction of P_4O_{10}. While the middle section of the monolith contains less phosphorus and has a higher fraction of metaphosphates. Moreover, closer to the outlet the phosphorus is more evenly distributed.

3. Materials and Methods

3.1. Catalyst Synthesis

The $Pt/BaO/Al_2O_3$ catalyst was synthesized using incipient wetness impregnation. To enhance the NO_x storage capacity of the chosen model catalyst, the impregnation of platinum on the support material was performed before incorporation of barium, which previously has shown beneficial to achieve high NO_x storage capacity of the catalyst [25]. Prior to the impregnation, the γ-alumina (Sigma-Aldrich) support was calcined for 2 h at 600 °C. Thereafter the γ-alumina support was impregnated with a platinum nitrate precursor (Heraeus platinum (II) nitrate; solution type K, batch: 12207), diluted with Milli-Q water (18 MΩ·cm) of the estimated volume targeting 2 wt.-% Pt. The impregnated support material was dried in air at 100 °C for 2 h and subsequently calcined in air at 550 °C for 2 h, starting from room temperature with a temperature increase of 5 °C/min. The calcined Pt/Al_2O_3 sample was then impregnated with a barium precursor (Sigma-Aldrich barium acetate, 99% A.C.S reagent, batch: 11415KA), dissolved in Milli-Q water in two steps also by incipient wetness impregnation, targeting a total of 16 wt.-% of BaO. The catalytic material was dried and calcined after each impregnation step under same conditions as for the impregnation of platinum.

3.2. Monolith Preparation

The catalytic material was coated on honeycomb-shaped ceramic monolith substrates (20 mm in length, 21 mm in diameter, a wall thickness of 0.106 mm and with 400 cpsi). To improve the adhesiveness, 10 wt.-% boehmite (Sasol disperal P2, product code: 538116) was mixed with the catalyst in a solution of 50 vol.-% Milli-Q water and 50 vol.-% ethanol. The monolith substrates were stepwise

dipped in the solution and dried at 90 °C until the target washcoat weight of 700 mg per monolith sample was reached. Thereafter, the catalysts were calcined at 550 °C for 2 h, starting from room temperature with a temperature increase of 5 °C/min.

3.3. Flow-Reactor Experiments

The flow-reactor experiments were carried out in a synthetic gas bench (SGB) reactor. The coated monolith samples were placed in a quartz tube, which was 750 mm in length and with an inner diameter of 22 mm. To prevent by-pass, quartz wool was wrapped around the monoliths. The gas flow and gas concentrations were regulated using mass flow controllers from Bronkhorst and water vapor was dosed using a Bronkhorst Controlled evaporation system (CEM) system. The quartz tube was placed in an electric heating coil and covered with insulation material, and the temperatures were measured by two thermocouples, one measuring and regulating the gas temperature before the catalyst and one measuring the catalyst temperature in a center channel of the monolith. An MKS Multigas 2030 FTIR spectrometer provided by MKS instruments, Andover, MA, USA was used to monitor the gas phase concentrations of NO, NO_2, N_2O, NH_3 and H_2O, and the total flow was 3500 mL/min, corresponding to 30,300 h^{-1} space velocity, with argon as carrier gas for all measurements. All lines and connections prior and after the reactor were heated to 200 °C, to prevent condensation.

To avoid sintering of platinum particles under the experiments, the coated monoliths were first H_2-treated in 1 vol.-% H_2, 5 vol.-% CO_2 and 5 vol.-% H_2O for 20 min at 500 °C and thereafter degreened at 600 °C, according to the following procedure. First the catalyst was exposed to the rich phase (400 vol.-ppm NO, 5 vol.-% CO_2, 1 vol.-% H_2 and 5 vol.-% H_2O with argon as carrier gas) for 60 min, followed by exposure to the lean phase (400 vol.-ppm NO, 5 vol.-% CO_2, 8 vol.-% O_2, and 5 vol.-% H_2O in argon) for 15 min. Subsequently, the catalyst was reduced in 1 vol.-% H_2, 5 vol.-% CO_2 and 5 vol.-% H_2O in Ar for 20 min at 600 °C.

The NO_x storage and reduction performance of the catalysts was studied at 300 and 400 °C using lean/rich cycling. At each temperature, two cycle segments consisting of five cycles in each segment were conducted. Cycle number 4 for all sequences is shown in the Figures. The gas composition of the lean phase was 400 vol.-ppm NO, 5 vol.-% CO_2, 8 vol.-% O_2, and 5 vol.-% H_2O. In the first lean/rich phase cycle segment, hydrogen was used as the reductant (1 vol.-% H_2, 400 vol.-ppm NO, 5 vol.-% CO_2 and 5 vol.-% H_2O) and in the second cycle segments propene was used as the reducing agent (0.1 vol.-% C_3H_6, 400 vol.-ppm NO, 5 vol.-% CO_2 and 5 vol.-% H_2O). For all cycles, the duration of the lean and rich phase were 4 and 1 min, respectively. Prior to the experiment at each temperature, the catalyst was pre-treated with 1 vol.-% H_2, 5 vol.-% CO_2 and 5 vol.-% H_2O for 15 min at 400 °C. This pre-treatment was also conducted for the phosphorus-exposed catalysts.

3.4. Phosphorous Exposure

The NO_x storage capacity of the coated monoliths was measured in the flow reactor before and after the exposure to phosphorus, using the procedure described in the previous section. The same reactor as described above was used for the phosphorous exposure, however using a separate reactor tube. In order to reduce surfaces for the evaporated phosphoric acid to stick to, the monolith was not wrapped in quartz wool during the phosphorous exposure. Phosphoric acid was introduced to the gaseous flow by a syringe pump connected to a Teflon pipe disposing the acid inside the quarts tube. The composition of the gas phase during the phosphorous exposure was 50 or 100 vol.-ppm evaporated phosphoric acid, 5 vol.-% H_2O, 8 vol.-% O_2 in argon as carrier gas, and the temperature was 200 °C. Two different phosphorous exposure conditions were studied in this work; in the first case the catalyst was exposed to 50 vol.-ppm phosphoric acid for 34 h, and in the second case the sample was exposed to 100 vol.-ppm for phosphoric acid for 34 h. This corresponds to an exposure of 1.7 and 3.4 g P/l catalyst, respectively. Note that high amounts of phosphorus passed through the catalyst without adsorption. These samples are denoted “50 ppm, 34 h” and “100 ppm, 34 h”, respectively. Note that new monolith samples were used for each poisoning condition.

3.5. XPS

To evaluate the oxidation state of phosphorus accumulated on the catalytic washcoat, an entire channel from the coated monolith was placed on a holder to measure the surface species of the washcoat. The use of a whole channel also enabled the identification of the axial position where measurements took place. The instrument used for the XPS analysis was a Perkin Elmer PHI 5000 ESCA system provided by PerkinElmer, Waltham, MA, USA equipped with an EDS elemental mapping system. The X-ray source for the XPS measurements was monochromatic Al Kα radiation at 1486.6 eV. Correction for charging was performed by normalizing the spectra using the C 1s peak at 284.6 eV [40] as reference. Furthermore, since normalizing will cause the largest peak being equal to 1, all spectra were divided by 1.1 for better visualization. Deconvolution of the P 2p peak from each sample was performed by fitting a Gaussian function to the experimental data, with subtraction of a linear baseline under both peaks. The peak positions were optimized according to the same procedure for both samples to achieve the lowest standard deviation and found to be 134.25, 135.5 and 132.5 eV for PO_3^-, P_4O_{10} and PO_4^{3-}, respectively.

3.6. N_2-Physisorption and ICP-AES

The specific surface area and pore volume of the samples were measured by N_2-physisorption isotherms at −195 °C and were collected using a TriStar 3000 gas adsorption analyzer. The inlet-, middle- and outlet section of the coated monoliths were crushed and grinded to powder form. Approximately 300 mg sample from each section was thermally dried at 90 °C in N_2 gas flow for 4 h and used for specific surface area and pore-volume measurements.

Powder samples from each section were used for elemental analysis by inductive coupled plasma atomic emission spectroscopy (ICP-AES), and the measurements were performed by ALS Scandinavia AB, Luleå, Sweden. The concentration of the measured phosphorus is reported as weight percentages.

3.7. ESEM

Environmental scanning electron microscopy (ESEM) was used to acquire an overview of the location of different elements over the catalytic washcoat. The instrument used to gain these images was a Quanta200 ESEM FEG from FEI, Hillsboro, OR, USA. An energy dispersive X-ray (EDX) system from Oxford Inca was equipped to the instrument to map the elements over scanned areas.

4. Conclusions

In the present study, a $Pt/Ba/Al_2O_3$ NO_x storage catalyst coated on a ceramic monolith substrate was exposed to two different phosphorus containing atmospheres for 34 h at 200 °C; 50 vol.-ppm H_3PO_4 + 8 vol.-% O_2 + 5 vol.-% H_2O and 100 vol.-ppm H_3PO_4 + 8 vol.-% O_2 + 5 vol.-% H_2O. The catalysts were characterized by N_2-physisorption, XPS, ESEM and ICP-AES, and the NO_x storage capacity was measured in flow reactor experiments.

The specific surface area and pore volume measurements, together with the elemental analysis by ICP-AES, showed a clear gradient distribution of phosphorous along the axial direction of the monolith. The phosphorus concentrations close to the inlet section of the sample were significantly higher compared to the middle and outlet section. The specific surface area and pore volume were found to be lower in the sections where the concentration of phosphorus was higher. At the outlet section, both the specific surface area and the pore volume were found to be comparable with those for the fresh sample, and the accumulated amount of phosphorus was only about 0.1 wt.-%, which can be compared with 2 wt.-% at the inlet section of the phosphorous exposed catalyst. Moreover, there was no significant difference between the different phosphorous concentrations, which indicates that the phosphorus concentration is not limiting the deposition of phosphorous on the catalyst, due to long exposure time.

Flow-reactor experiments showed that the NO_x storage capacity of $Pt/BaO/Al_2O_3$ decreased with presence of phosphorous species on the catalyst. The results also showed that the formation of N_2 decreased after the exposure to phosphorous, in favour of ammonia production. Furthermore, the formation of N_2O decreased after the phosphorus exposure. The increased ammonia production can be explained by the fact that the outlet ammonia concentration is dependent on three reactions over the catalyst: (i) the formation of ammonia from NO in the inlet gas; (ii) formation of ammonia from stored NO_x; and (iii) the consumption of ammonia through the selective catalytic reduction by the reaction with the stored nitrates. Since the amount of stored nitrates is lower for the phosphorus exposed sample, it means that less ammonia is produced in reaction (ii), but simultaneously less ammonia is consumed in reaction (iii). Since there is more ammonia in total, it means that the SCR reaction is more influenced by the phosphorus poisoning than the ammonia formation from the stored nitrates.

The XPS analysis showed that phosphorus exposure resulted in the formation of different species depending on the axial location of the washcoat. At the inlet section of the catalyst, where most of the phosphorus was accumulated, the dominating phosphorous species was found to be P_4O_{10} while further along the axial direction metaphosphates (PO_3^-) was the dominating species. From the ESEM and EDX analysis it could be concluded that most phosphorus, close to the inlet of the catalyst, was located at the washcoat surface. At the outlet, only a small amount of phosphorus could be detected by SEM-EDX, however, it was more diffused into the washcoat. To summarize, the results from XPS and SEM indicate that the accumulation of phosphorus differs between the front and the back of the monolith catalyst.

Acknowledgments: This work was conducted at the Competence Centre for Catalysis (KCK) hosted by Chalmers University of Technology and financially supported by the Swedish Energy Agency, Chalmers and the member companies AB Volvo, ECAPS AB, Haldor Topsøe A/S, Scania CV AB, Volvo Car Corporation AB, and Wärtsilä Finland Oy. KCK is greatly acknowledged for their financial support. Lars Ilver is gratefully acknowledged for the assistance with XPS measurements.

Author Contributions: R.J. and L.O. conceived and designed the experiments; R.J. performed the experiments; R.J., O.M., M.S., E.O., M.B. and L.O. analyzed the data; L.I. and J.W. contributed analysis tools; R.J. wrote the paper.

Conflicts of Interest: The authors declare no conflict of interest.

References

1. Guerreiro, C.; Gonzalez Ortiz, A.; de Leeuw, F.; Viana, M.; Horalek, J. *Air Quality in Europe—2016 Report*; European Environment Agency (EEA): Copenhagen, Denmark, 2016; ISBN 9789292138240.
2. Takahashi, N.; Shinjoh, H.; Iijima, T.; Suzuki, T.; Yamazaki, K.; Yokota, K.; Suzuki, H.; Miyoshi, N.; Matsumoto, S.; Tanizawa, T.; et al. The new concept 3-way catalyst for automotive lean-burn engine: NO_x storage and reduction catalyst. *Catal. Today* **1996**, *27*, 63–69. [CrossRef]
3. Epling, W.S.; Campbell, L.E.; Yezerets, A.; Currier, N.W.; Parks, J.E. Overview of the fundamental reactions and degradation mechanisms of NO_x storage/reduction catalysts. *Catal. Rev. Sci. Eng.* **2004**, *46*, 163–245. [CrossRef]
4. Matsumoto, S. Recent advances in automobile exhaust catalysts. *Catal. Today* **2004**, *90*, 183–190. [CrossRef]
5. Fridell, E.; Skoglundh, M.; Westerberg, B.; Johansson, S.; Smedler, G. NO_x Storage in Barium-Containing Catalysts. *J. Catal.* **1999**, *183*, 196–209. [CrossRef]
6. Lindholm, A.; Currier, N.W.; Li, J.; Yezerets, A.; Olsson, L. Detailed kinetic modeling of NO_x storage and reduction with hydrogen as the reducing agent and in the presence of CO_2 and H_2O over a Pt/Ba/Al catalyst. *J. Catal.* **2008**, *258*, 273–288. [CrossRef]
7. Lindholm, A.; Currier, N.W.; Fridell, E.; Yezerets, A.; Olsson, L. NO_x storage and reduction over Pt based catalysts with hydrogen as the reducing agent. Influence of H_2O and CO_2. *Appl. Catal. B Environ.* **2007**, *75*, 78–87. [CrossRef]
8. Lindholm, A.; Sjövall, H.; Olsson, L. Reduction of NO_x over a combined NSR and SCR system. *Appl. Catal. B Environ.* **2010**, *98*, 112–121. [CrossRef]

9. Nova, I.; Castoldi, L.; Lietti, L.; Tronconi, E.; Forzatti, P.; Prinetto, F.; Ghiotti, G. NO_x adsorption study over Pt-Ba/alumina catalysts: FT-IR and pulse experiments. *J. Catal.* **2004**, *222*, 377–388. [CrossRef]
10. Partridge, W.P.; Choi, J.S. NH_3 formation and utilization in regeneration of $Pt/Ba/Al_2O_3$ NO_x storage-reduction catalyst with H_2. *Appl. Catal. B Environ.* **2009**, *91*, 144–151. [CrossRef]
11. De Abreu Goes, J.E.; Olsson, L.; Berggrund, M.; Kristoffersson, A.; Gustafson, L.; Hicks, M. Performance Studies and Correlation between Vehicle- and Rapid-Aged Commercial Lean NO_x Trap Catalysts. *SAE Int. J. Engines* **2017**, *10*. [CrossRef]
12. Bartholomew, C.H. Mechanism of catalyst deactivation. *Appl. Catal. A Gen.* **2001**, *212*, 17–60. [CrossRef]
13. Bunting, B.G.; More, K.; Lewis, S.; Toops, T. Phosphorous Poisoning and Phosphorous Exhaust Chemistry with Diesel Oxidation Catalysts. *SAE Tech. Pap.* **2005**. [CrossRef]
14. Sedlmair, C.; Seshan, K.; Jentys, A.; Lercher, J.A. Studies on the deactivation of NO_x storage-reduction catalysts by sulfur dioxide. *Catal. Today* **2002**, *75*, 413–419. [CrossRef]
15. Huang, H.Y.; Long, R.Q.; Yang, R.T. A highly sulfur resistant $Pt-Rh/TiO_2/Al_2O_3$ storage catalyst for NO_x reduction under lean-rich cycles. *Appl. Catal. B Environ.* **2001**, *33*, 127–136. [CrossRef]
16. Umeno, T.; Hanzawa, M.; Hayashi, Y.; Hori, M. Development of New Lean NO_x Trap Technology with High Sulfur Resistance. *SAE Tech. Pap.* **2014**. [CrossRef]
17. Le Phuc, N.; Corbos, E.C.; Courtois, X.; Can, F.; Marecot, P.; Duprez, D. NO_x storage and reduction properties of $Pt/CexZr_{1-x}O_2$ mixed oxides: Sulfur resistance and regeneration, and ammonia formation. *Appl. Catal. B Environ.* **2009**, *93*, 12–21. [CrossRef]
18. Darr, S.T.; Choksi, R.A.; Hubbard, C.P.; Johnson, M.D.; Mccabe, R.W.; Co, F.M. Effects of Oil-Derived Contaminants on Emissions from TWC-Equipped Vehicles. *SAE Tech. Pap.* **2000**. [CrossRef]
19. Sumida, H.; Koda, Y.; Sadai, A.; Ichikawa, S.; Kyogoku, M.; Takato, M.; Miwa, Y. Analysis of Phosphorus Poisoning on Exhaust Catalysts from Compact-Class Vehicle. *SAE Tech. Pap.* **2004**. [CrossRef]
20. Rokosz, M.J.; Chen, A.E.; Lowe-Ma, C.K.; Kucherov, A.V.; Benson, D.; Paputa Peck, M.C.; McCabe, R.W. Characterization of phosphorus-poisoned automotive exhaust catalysts. *Appl. Catal. B Environ.* **2001**, *33*, 205–215. [CrossRef]
21. Angove, D.E.; Cant, N.W. Position dependent phenomena during deactivation of three-way catalytic converters on vehicles. *Catal. Today* **2000**, *63*, 371–378. [CrossRef]
22. Ball, D.J.; Mohammed, A.G.; Schmidt, W.A. Application of Accelerated Rapid Aging Test (RAT) Schedules with Poisons: The Effects of Oil Derived Poisons, Thermal Degradation and Catalyst Volume on FTP Emissions. *SAE Tech. Pap.* **1997**. [CrossRef]
23. Guevremont, J.M.; Guinther, G.; Jao, T.; Herlihy, T.; White, R.; Howe, J. Total Phosphorus Detection and Mapping in Catalytic Converters. *Powertrain Fluid Syst. Conf. Exhib.* **2007**. [CrossRef]
24. Cabello Galisteo, F.; López Granados, M.; Martín Alonso, D.; Mariscal, R.; Fierro, J.L.G. Loss of NO_x storage capacity of $Pt-Ba/Al_2O_3$ catalysts due to incorporation of phosphorous. *Catal. Commun.* **2008**, *9*, 327–332. [CrossRef]
25. Lindholm, A.; Currier, N.W.; Dawody, J.; Hidayat, A.; Li, J.; Yezerets, A.; Olsson, L. The influence of the preparation procedure on the storage and regeneration behavior of Pt and Ba based NO_x storage and reduction catalysts. *Appl. Catal. B Environ.* **2009**, *88*, 240–248. [CrossRef]
26. Sharma, M.; Harold, M.P.; Balakotaiah, V. Analysis of periodic storage and reduction of NO_x in catalytic monoliths. *Ind. Eng. Chem. Res.* **2005**, *44*, 6264–6277. [CrossRef]
27. Lietti, L.; Nova, I.; Forzatti, P. Role of ammonia in the reduction by hydrogen of NO_x stored over $Pt-Ba/Al_2O_3$ lean NO_x trap catalysts. *J. Catal.* **2008**, *257*, 270–282. [CrossRef]
28. Nova, I.; Castoldi, L.; Lietti, L.; Tronconi, E.; Forzatti, P. How to control the selectivity in the reduction of NO_x with H_2 over $Pt-Ba/Al_2O_3$ Lean NO_x Trap catalysts. *Top. Catal.* **2007**, *42–43*, 21–25. [CrossRef]
29. Tonkyn, R.G.; Disselkamp, R.S.; Peden, C.H.F. Nitrogen release from a NO_x storage and reduction catalyst. *Catal. Today* **2006**, *114*, 94–101. [CrossRef]
30. Olsson, L.; Fridell, E.; Skoglundh, M.; Andersson, B. Mean field modelling of NO_x storage on $Pt/BaO/Al_2O_3$. *Catal. Today* **2002**, *73*, 263–270. [CrossRef]
31. Clayton, R.D.; Harold, M.P.; Balakotaiah, V. Selective catalytic reduction of NO by H_2 in O_2 on $Pt/BaO/Al_2O_3$ monolith NO_x storage catalysts. *Appl. Catal. B Environ.* **2008**, *81*, 161–181. [CrossRef]

32. Choi, J.-S.; Partridge, W.P.; Pihl, J.A.; Kim, M.-Y.; Kočí, P.; Daw, C.S. Spatiotemporal distribution of NO_x storage and impact on NH_3 and N_2O selectivities during lean/rich cycling of a Ba-based lean NO_x trap catalyst. *Catal. Today* **2012**, *184*, 20–26. [CrossRef]
33. Bamwenda, G. The role of the metal during NO_2 reduction by C_3H_6 over alumina and silica-supported catalysts. *J. Mol. Catal. A Chem.* **1997**, *126*, 151–159. [CrossRef]
34. Ji, Y.; Easterling, V.; Graham, U.; Fisk, C.; Crocker, M.; Choi, J.S. Effect of aging on the NO_x storage and regeneration characteristics of fully formulated lean NO_x trap catalysts. *Appl. Catal. B Environ.* **2011**, *103*, 413–427. [CrossRef]
35. Moulder, J.F.; Stickle, W.; Sobol, P.E.; Bomben, K.D. *Handbook of X-ray Photoelectron Spectroscopy*; Perkin Elmer Corporation: Eden Prairie, MN, USA, 1992.
36. Andonova, S.; Vovk, E.; Sjöblom, J.; Ozensoy, E.; Olsson, L. Chemical deactivation by phosphorous under lean hydrothermal conditions over Cu/BEA NH_3-SCR catalysts. *Appl. Catal. B Environ.* **2014**, *147*, 251–263. [CrossRef]
37. Shwan, S.; Jansson, J.; Olsson, L.; Skoglundh, M. Chemical deactivation of Fe-BEA as NH_3-SCR catalyst-Effect of phosphorous. *Appl. Catal. B Environ.* **2014**, *147*, 111–123. [CrossRef]
38. Andersson, J.; Antonsson, M.; Eurenius, L.; Olsson, E.; Skoglundh, M. Deactivation of diesel oxidation catalysts: Vehicle- and synthetic aging correlations. *Appl. Catal. B Environ.* **2007**, *72*, 71–81. [CrossRef]
39. Beck, D.; Monroe, D.; Di Maggio, C.; Sommers, J. Impact of Oil-Derived Catalyst Poisons on FTP Performance of LEV Catalyst Systems. *SAE Trans.* **1997**. [CrossRef]
40. Yamashita, T.; Hayes, P. Analysis of XPS spectra of Fe^{2+} and Fe^{3+} ions in oxide materials. *Appl. Surf. Sci.* **2008**, *254*, 2441–2449. [CrossRef]